JAIST Repository
https://dspace.jaist.ac.jp/

Title	Dependences of deposition rate and OH content on concentration of added trichloroethylene in low-temperature silicon oxide films deposited using silicone oil and ozone gas
Author(s)	Horita, Susumu; Jain, Puneet
Citation	Japanese Journal of Applied Physics, 57(3S1): 03DA02-1-03DA02-7
Issue Date	2018-01-23
Type	Journal Article
Text version	author
URL	http://hdl.handle.net/10119/15734
Rights	This is the author's version of the work. It is posted here by permission of The Japan Society of Applied Physics. Copyright (C) 2018 The Japan Society of Applied Physics. Susumu Horita and Puneet Jain, Japanese Journal of Applied Physics, 57(3S1), 2018, 03DA02-1-03DA02-7. http://dx.doi.org/10.7567/JJAP.57.03DA02
Description	

JAIST
JAPAN
ADVANCED INSTITUTE OF
SCIENCE AND TECHNOLOGY

Japan Advanced Institute of Science and Technology

Dependences of deposition rate and OH content on concentration of added trichloroethylene in low-temperature silicon oxide films deposited using silicone oil and ozone gas

Susumu Horita* and Puneet Jain
School of Materials Science, Japan Advanced Institute of Science and Technology, Nomi, Ishikawa 923-1292, Japan
*E-mail: horita@jaist.ac.jp

Abstract

We investigated the dependences of the deposition rate and residual OH content of SiO_2 films on the concentration of trichloroethylene (TCE), which was added during deposition at low temperatures of 160-260 ^{o}C with the reactant gases of silicone oil (SO) and O_3. The deposition rate depends on the TCE concentration and is minimum at a concentration of ~0.4 mol/m^3 at 200 ^{o}C. The result can be explained by surface and gas-phase reactions. Experimentally, we also revealed that the thickness profile is strongly affected by gas-phase reaction, in which the TCE vapor was blown directly onto the substrate surface, where it mixed with SO and O_3. Furthermore, it was found that adding TCE vapor reduces residual OH content in the SiO_2 film deposited at 200 ^{o}C because TCE enhances the dehydration reaction.

1. Introduction

Low-temperature deposition of silicon oxide films is needed for the fabrication of not only thin-film transistors (TFTs) on non-heat-resistant substrates[1] but also interlayer dielectrics (ILD) in size-minimizing integrated circuits to suppress the disconnection of the interconnect metal, the redistribution of the dopant, and defect generation in the fabricated underlayer.[2] For low-temperature deposition, plasma-enhanced chemical vapor deposition (PECVD) has been widely used in practice.[1,3-6] However, it requires an expensive system consisting of vacuum equipment and high power supply. Additionally, tetraethylorthosilicate [TEOS; $Si(OC_2H_5)_4$] vapor is commonly used as a deposition gas source.[3-5] However, we previously reported on the low-temperature deposition of Si oxide films using silicone oil (SO) vapor as a deposition source and ozone (O_3) gas at temperatures of 200 - 350 ^oC at atmospheric pressure without vacuum or pumping systems.[7,8] SO has advantages over TEOS; the price per unit volume of SO is lower than that of TEOS by about one order, and silicone is not only markedly thermally stable but also a safe material, whereas TEOS is toxic especially to the human eye and throat.[9]

However, the rate of Si oxide film deposition using SO is very low at less than 5 nm/min,[8] which is not favorable for industrial application. To overcome this problem, we have reported recently that adding some amount of trichloroethylene (C_2HCl_3; TCE) vapor markedly increases the deposition rate to more than 3 times that without TCE during deposition in combination with SO and O_3 at deposition temperatures lower than 200 ^oC.[10] The increase in the deposition rate is caused by TCE-enhanced dehydration reaction between silanols of the precursors and OH bonds terminated at the surface of the substrate or deposited film, i.e.,

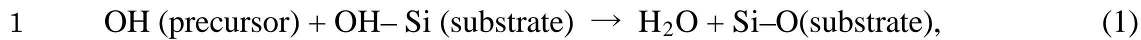

$$OH\ (precursor) + OH\text{–}Si\ (substrate) \rightarrow H_2O + Si\text{–}O(substrate), \quad (1)$$

as determined on the basis of the previous reports on the deposition mechanism of the $TEOS/O_3$ system.[11-14] TCE may be decomposed into H and C among others because of the highly reactive O_3, and hydrochloric acid can be formed. Commonly, an acid is used as a catalyst to enhance the dehydration reaction in an organic chemical solution, e.g., in the Fischer esterification reaction.[15]

However, contrary to expectation, when the deposition temperature is increased to more than 200 ^{o}C, the deposition rate is suppressed or reduced despite the enhancement of the dehydration reaction.[10] This can be explained on the basis of the gas-phase and surface reactions.[16-19] The gas phase reaction is a chemical reaction that occurs between gaseous reactants or SO + O_3 near the substrate surface but not on it. Thus, owing to this reaction, some of the reactants are consumed without contributing to film deposition, which can reduce film deposition rate. The surface reaction is a chemical reaction that occurs between the gaseous reactants on active sites of the substrate surface, which contributes to film deposition.

On the other hand, it remains unclarified how the TCE concentration in reactant gas affects deposition rate. This investigation result will provide us with a method to increase the deposition rate further. Moreover, it is expected that the dehydration reaction enhancement due to TCE produces a low residual OH content in the deposited films. It has been reported that OH bond formation in low-temperature Si oxide films leads to the serious problems of high leakage current and low breakdown voltage.[8,20-22]. Generally, low-temperature SiO_2 films prepared by CVD methods with organic silicon sources such as TEOS are more likely to contain a large amount of OH bonds when no special treatment is carried out, e.g., postdeposition annealing. Recently, we have

reported some information on the TCE concentration dependence of deposition rate and the effect of TCE in reducing OH content in low-temperature SiO_2 films.[23] However, the results and discussion are insufficient to further improve the deposition rate and reduce the residual OH content. Therefore, in this paper, with the addition of new data, the results are comprehensively reported and are discussed deeply from the viewpoints of the surface and gas-phase reactions of the reactants SO, O_3, and TCE. Furthermore, as a verification experiment for the gas-phase reaction, we blew TCE vapor on the substrate surface directly, where it mixed with the other reactant gases SO and O_3 flowing from elsewhere. Hereafter, this is referred to as “TCE direct flow”. Then, we measured film thickness and refractive index profiles at different distances from the outlet of the TCE direct flow. The profiles clearly show a trace of the gas-phase reaction.

2. Experimental procedure

Figure 1(a) shows a schematic diagram of the deposition system used in this study. The system has a vertical reactor for atmospheric-pressure (AP) CVD. The details are mentioned in a previous paper.[10] The SO used was decamethylcyclopentasiloxane ($C_{10}H_{30}O_5Si_5$) heated to 50 ^{o}C using a mantle heater, and its vapor was generated by bubbling with N_2 gas. The flow rates of N_2 gas for the SO vapor, F_{N2}(SO), were 0.25 and 0.35 lm (liters per minute at 25 ^{o}C). O_3 was generated using a silent electric discharge from 99.9995% O_2 gas at a flow rate of 0.50 lm and the O_3 concentration was ~145 g/m^3. The TCE vapor was generated by bubbling with N_2 gas, and it was then made to flow to one of the two lines, as shown in Fig. 1(a). One line led to the bottom of the chamber equipped with the SO vapor and O_3 + O_2 lines, and the other led to the

1 substrate surface directly, i.e., TCE direct flow. In this case, the 1/4-in. diameter
2 stainless tube was set ~5 mm above the substrate, as shown in Fig. 1(b). The gas flow
3 direction to the chamber bottom or the substrate surface was controlled using the
4 three-way valve shown in Fig. 1(a). The distance between the showerhead and the
5 substrate was ~100 mm. The films were deposited for 10 min at substrate temperatures
6 of 160-260 ^{o}C. The TCE concentration in the reactive chamber was varied from ~0.10
7 to ~0.7 mol/m^3 by adjusting both the TCE solution temperature from 5 to 32 ^{o}C and the
8 N_2 gas flow rate, F_{N2}(TCE), from 0.03 to 0.1 lm for bubbling TCE. For TCE direct flow,
9 the TCE flow rate was 0.0034 or 0.00065 lm. The TCE concentration on the substrate
10 surface is not uniform in this case because the TCE vapor immediately and randomly
11 diffuses inside the reaction chamber after its release from the tube. Assuming that the
12 TCE vapor is distributed uniformly in the reaction chamber, the concentrations at the
13 TCE flow rates of 0.0034 and 0.00065 lm are calculated to be 0.15 and 0.03 mol/m^3,
14 respectively. The detailed calculations of the TCE concentration and flow rate are
15 described in Appendix.
16 Substrates were n-type (111) single crystals with resistivities of 5–15 Ωcm. Before
17 setting a substrate on a holder, it was chemically cleaned in a hot acid solution and
18 dipped in a dilute HF solution to remove Si oxide. The thicknesses and refractive
19 indexes of the as-deposited films were measured by ellipsometry using a He-Ne laser
20 beam with a wavelength of 632.8 nm. For the TCE bottom flow method, 3 points were
21 measured on a 20×10 mm^3 substrate, which were near each edge and the center along
22 the length of the substrate. For the TCE direct flow, points every 1.5 ~ 3.0 mm apart
23 were measured on a ~20×60 mm^3 substrate along the length. The molecular structures
24 of the as-deposited films were analyzed from Fourier transform infrared spectroscopy

(FT-IR) spectra with a resolution of 1 cm^{-1}.

3. Results

Figure 2 shows the typical FT-IR spectra of the silicon oxide films deposited at 200 ^{o}C with TCE (top and middle curves) and without TCE (bottom curve) as a reference. The F_{N2}(SO) values are 0.25 (middle curve) and 0.35 lm (upper and bottom curves), and the TCE concentration is 0.25 mol/m^3 for both F_{N2}(SO) values. The peaks at ~800 and 1070 cm^{-1} are identified as absorptions due to the bending (TO_2) and asymmetric stretching (TO_3) modes of the Si–O–Si bond, respectively.[24-27] This indicates that the silicon oxide films contain few hydrocarbon bonds from the deposition source of SO and that their chemical composition is almost the same as that of thermal oxide films. However, peaks due to the Si-OH bonds appear at around 960 and 3650, and those due to the H-OH bonds appear at ~3300 cm^{-1}, which are very often observed in films deposited by common low-temperature deposition methods using organic silicon deposition sources without any post-treatment.[11,20,21,28-30] By comparing the spectra with and without TCE at F_{N2}(SO) = 0.35 lm, it can be seen clearly that the peak intensities due to the Si-O-Si bond are markedly higher with TCE than without TCE. This is valid even for the lower F_{N2}(SO) of 0.25 lm, which supplies less Si source than F_{N2}(SO) = 0.35 lm. This result suggests that adding TCE should increase the deposition rate of Si oxide films markedly.

Figure 3 shows the temperature dependences of deposition rates obtained with (closed circles and triangles) and without (open circles) TCE (as a reference), where the temperatures range from 160 to 260 ^{o}C and the TCE concentration is 0.25 mol/m^3. The F_{N2} (SO) values with (closed circles and triangles) and without TCE (open circles) are

0.25 and 0.35, and 0.35 lm, respectively. The data plots and error bars indicate the averages and ranges of deposition rate, respectively, among all the measurement points. It can be seen from Fig. 3 that, at temperatures lower than 220 ^{o}C, the deposition rate is higher with TCE than without TCE. For the samples with TCE, the deposition rates at F_{N2}(SO) = 0.35 lm are always larger than those at F_{N2}(SO) = 0.25 lm at any deposition temperature because the Si source supply for the former is larger than that for the latter. Also, the deposition rates with TCE at both F_{N2}(SO) values saturate at higher deposition temperatures while that without TCE increases rapidly with temperature. These phenomena are almost the same as those observed in a previous study where TCE concentration was not controlled, which can be explained by surface and gas-phase reactions.[10)]

Figure 4 shows the dependences of deposition rate on TCE concentration for the N_2(SO) flow rates of 0.35 (circles) and 0.25 (triangles) lm,[23)] where the data plot marks and error bars have the same meanings as those in Fig. 3. The deposition rate of ~4.4 nm/min without TCE is shown as a broken solid line for reference. It is found from this result that the deposition rate with TCE at F_{N2}(SO) = 0.35 lm at any TCE concentration is more than twice that without TCE. Even at the smaller F_{N2}(SO) = 0.25 lm, the deposition rates with TCE are higher than that without TCE. It can be seen, also, that the deposition rates depend on the TCE concentration, and the TCE concentration of the minimum deposition rate is approximately 0.4 mol/m^3. This result indicates that the TCE concentration affects the chemical reaction between SO and O_3. This is discussed in more detail in Sect. 4.

To quantify OH content in the deposited SiO_2 films, we used peak intensity ratios at ~3400 and ~1070 cm^{-1} in the FT-IR spectra, which are representative of the H-OH and

Si-O-Si bond vibration modes, respectively. The intensity ratio gives us the relative number of OH bonds in deposited SiO_2 films. Figure 5 shows the deposition rate dependence of relative OH content in the deposited films.[23)] The closed triangles and circles under the broken line show the data for $F_{N2}(SO)$ = 0.25 and 0.35 lm, respectively, with TCE, and the open circle enclosed with a broken circle shows the data for deposition without TCE. As can clearly be seen from Fig. 5, the OH contents with TCE are much smaller than that without TCE. This means that the addition of TCE to the gas source is very effective in reducing OH content in the deposited SiO_2 films because of TCE-enhanced dehydration reaction. Furthermore, it can notice that the OH content in the SiO_2 films deposited with TCE is roughly proportional to the deposition rate although the data are somewhat scattered. Also, the data for deposition with TCE can be divided roughly into two groups in terms of the source gas flow rate, i.e., $F_{N2}(SO)$ = 0.25 and 0.35 lm. Generally, the OH content for the $F_{N2}(SO)$ = 0.35 lm group is larger than that for the 0.25 lm group since the deposition rate for $F_{N2}(SO)$ = 0.35 lm is on average about 1.5 times higher than that for $F_{N2}(SO)$ = 0.25 lm. The residual OH bonds in a Si oxide film are mainly due to the nondehydration reaction between silanols of the precursors and OH bonds terminated at the substrate surface, which has a statistical thermodynamic possibility of occurring. The probability of the dehydration reaction may be reduced if the deposition rate increases because of a shorter reaction time. Therefore, the number of unreacted OH bonds or the residual OH content in the deposited film is approximately proportional to the deposition rate as shown in Fig. 5. Furthermore, no TCE concentration dependence of residual OH content was observed clearly, and the data are not shown here. This is probably because OH content is governed mainly by deposition rate as shown in Fig. 5.

4. Discussion

As mentioned above, TCE enhances the dehydration reaction so that Si oxide formation is promoted on the substrate surface even at temperatures lower than 200 ^{o}C. This effect may promote the dehydration reaction in the gas phase during the transport of reactant gases and precursors toward the substrate. In order to confirm whether the gas-phase reaction really does occur in our experiment or not, we performed the experiment shown in Fig. 1(b). As expected, film thickness decreases with the distance x from the outlet of the tube exponentially because of gas diffusion. Figure 6 shows the film thickness (left) and refractive index (right) profiles as functions of the distance x from the tube outlet for 10 min deposition at 200 ^{o}C, where F_{N2}(SO) = 0.35 lm, and the TCE flow rates, F_{TCE}, are 0.0034 (circles) and 0.00065 (triangles) lm. It can be seen that, under both conditions, the film thicknesses generally decreases with distance as predicted. The thickness for F_{TCE} = 0.0034 lm is larger than that for F_{TCE} = 0.00065 lm in spite of the same supply rate of the SO deposition source, F_{N2}(SO) = 0.35 lm, because the supply of TCE is much larger. In both cases, the asymptotic values at large distances (x) appear to approach about 50 nm, which is close to the value obtained without TCE, as shown in Figs. 3 and 4. This is probably because, at large distances, the TCE concentration is much reduced because of the random and fast diffusion of TCE in the chamber. However, the thickness profile with the higher TCE flow rate has two peaks at x = ~15 and ~30 mm while that with the lower TCE flow rate shows a curve that smoothly declines with x. On the other hand, the distance dependence of the refractive index appears similar to that of film thickness with the exception that the refractive index is much lower around the first peak position of the film thickness for F_{TCE} =

0.0034 lm. According to the Lorentz-Lorenz model,[31,32] the refractive index is directly proportional to the density of the film. Since the refractive indexes shown in Fig. 6 are lower than 1.46 of thermal SiO_2, it is considered that the film densities are also lower. In particular, the refractive indexes in the region of the thicker film, i.e., x = 10 ~ 20 mm, are less than 1.3, which means that the film density is considerably lower in this region than in the other regions. This is experimentally supported by Figs. 7(a) and 7(b), which show Nomarski optical micrographs of the surface regions at x = ~10 and ~40 mm, respectively, in the sample with the TCE flow rate of 0.0034 lm in Fig. 6. From Fig. 7, it can be seen clearly that the surface at x = ~10 mm is much rougher than that at x = ~40 mm. This result seems to correspond well to the refractive index behavior shown in Fig. 6. Formation of surface roughness at x = ~10 mm is further discussed later.

Now, we focus our discussion on the two peaks in deposition rate for F_{TCE} = 0.0034 lm. O_3 is decomposed thermally into O_2+O at temperatures of more than 150 ^oC,[8] which is highly possible near the substrate owing to heat irradiation from the holder, which is heated at 200 ^oC. Thus chemically, very active O atoms react with the $–CH_3$ side groups of SO in the gas phase during the transport from the chamber bottom, and the $–CH_3$ side groups are substituted with hydroxyl –OH groups, and the silanol bonds of Si–OH cover the sides of siloxane chains. Then, precursors are formed. Furthermore, owing to the effect of TCE, it is possible that the dehydration reaction of OH between some precursors occurs in the gas phase, and SiO_2 particles are formed during the transport of the reactant gases before reaching the substrate. Increasing TCE concentration must promote the formation of SiO_2 particles in the gas phase. This gas-phase reaction is expressed by

1 Si-OH (precursor) + Si-OH (precursor) → H_2O + Si-O-Si. (2)

2 Near the outlet tube, i.e., x = 0 to 15 mm, the TCE concentration is so high that heavy
3 condensation or contraction of the precursors due to dehydration reactions between
4 them occurs not only on the substrate surface but also in the gas phase as mentioned
5 above. Therefore, SiO_2 particles are deposited loosely on the substrate, and then the
6 film thickness becomes much larger as shown in Fig. 6. Also, the surface becomes too
7 rough as shown in Fig. 7(a), so that the density of the deposited Si oxide film is much
8 lower than that of thermal silicon oxide as well as the refractive index. Accompanying
9 this complex dehydration reaction, the density of the precursor in the gas phase is much
10 reduced, which induces fast diffusion flow of the precursor from the region at x = ~25
11 mm toward the tube outlet. As a result, the precursor density at x = ~25 mm is also
12 much reduced, and the film thickness profile has a minimum and a second peak at x =
13 25 and 30 mm, respectively, as shown in Fig. 6. This phenomenon might be hardly
14 explained by the surface reaction without the involvement of the gas-phase reaction
15 because high condensation and diffusion speeds of the precursor are needed for the
16 formation of the two peaks in the thickness profile. Therefore, we can say that the
17 gas-phase reaction is highly involved in the deposition mechanism when TCE is used.

18 Next, we discuss the TCE concentration dependence of deposition rate, as shown in
19 of Fig. 4, in particular, the minimum value and the fluctuation in deposition rate
20 behaviors in the TCE concentration range from 0.2 to 0.5 mol/m^3. Figure 8 shows a
21 schematic model of SiO_2 film deposition with emphasis on the TCE-enhanced
22 dehydration reaction at the substrate surface. The –OH groups on the surface are
23 eliminated by the dehydration reaction with the –OH groups of the precursors, and then
24 a $[–Si–O–Si–]_n$ network is constructed on the substrate and the deposition of Si oxide

films continues. The elimination of OH groups is markedly promoted by adding TCE vapor, which leads to an increase in deposition rate, as shown above. However, if TCE concentration increases, e.g., to more than 0.2 mol/m^3, the gas-phase reaction may occur at non-negligible levels from the viewpoint of film deposition on the substrate. When the amount of SiO_2 formation due to the gas-phase reaction is much smaller than the amount needed for deposition thickness, we do not need to take the gas-phase reaction into account for the deposition model, and vice versa. Also, since the TCE gas flows from the chamber bottom, most SiO_2 particles formed in the gas phase probably do not contribute to film deposition on the substrate because of random scattering caused by the N_2 carrier gas and unreacted O_2 gas, with which the reaction chamber is almost filled. Furthermore, the SiO_2 particles have few OH bonds that act as a binding agents on the substrate surface through the dehydration reaction. This situation is different from the direct TCE flow shown in Figs. 1(b) and 6 because the distance from the SiO_2 formation location to the substrate in Figs. 1(a) and 4 is much larger than that in the direct TCE flow, which is less than 5 mm in Fig. 6. Therefore, the non-negligible amount of SiO_2 produced by the gas-phase reaction increases with the TCE concentration from 0.2 mol/m^3, which causes a decrease in deposition rate, as shown in Fig. 4. However, when the TCE concentration becomes greater than about 0.4 mol/m^3, the reversal reaction of Eq. (2) (or Si-OH + Si–OH $\leftarrow$ H_2O + Si–O-Si) would occur more frequently according to the chemical equilibrium formula

$$\frac{[\mathrm{H_2O}][\text{Si-O-Si}]}{[Si{-}OH]^2} = K, \tag{3}$$

where K is constant. Thus, since the dehydration reaction and consumption of precursors are suppressed to some level, even after increasing the TCE concentration further, precursors that are not reacted before arriving at the substrate can contribute to

the surface reaction. As a result, the deposition rate increases gradually with TCE concentration, as shown in Fig. 4.

The above discussion on Fig. 4 is examined quantitatively. When the TCE concentration was 0.2 mol/m^3, the concentrations of SO and O_3 used in the reaction chamber are calculated to be about 0.025 and 1.7 mol/m^3, respectively. The calculation details are provided in Appendix. According to the chemical reaction between SO and O_3 given in Appendix [Eq. (A·5)], the O_3 concentration (C_{O3}) of 1.7 mol/m^3 is sufficient for reaction with SO at the concentration (C_{SO}) of 0.025 mol/m^3 because the minimum required C_{O3} is estimated as $0.025 \times 40 = 1.0$ mol/m^3. Next, the necessary TCE concentration for the dehydration reaction is estimated roughly for $C_{SO} = 0.025$ mol/m^3. Here, we assume that all 10 OH bonds of one precursor molecule shown in Fig. 8 undergo dehydration reactions and that the reaction per one OH bond is assisted by one HCl molecule produced from one TCE molecule. The estimated value is 0.25 mol/cm^3 and roughly near the TCE concentration of 0.2 mol/m^3 at which the deposition rate starts decreasing, as shown in Fig. 4. Therefore, it can be said that the above discussion on Fig. 4 is reasonable qualitatively.

Figure 6 shows that, with a deposition time of 10 min, the refractive index slightly decreases with decreasing film thickness or deposition rate except for the region of rates higher than ~15 nm/min. Also, it is found actually that, in the samples shown in Fig. 4, the refractive index decreases with decreasing deposition rate, which is not shown here but is almost similar to the behavior shown in Fig. 6. Here, we will briefly discuss two possible mechanisms for this as follows: In addition to the gas-phase reaction, we can consider the possibility that a –OH-terminated Si on the film is released or desorbed from the surface by thermal energy, and this probability would increase with time

assuming no overlayer deposition. Since a surface site without a –OH bond has a dangling bond, it may become a defective hole or void after successive deposition of an overlayer. That is, the –OH bonds are removed by not only dehydration reactions but also thermal desorption with a specific time constant. Therefore, the lower deposition rate induces a larger volume of voids or lower density of the deposited film so that the refractive index is reduced. The other possible mechanism involves surface roughness. The surface of the deposited Si oxide film is not perfectly smooth, and it might have a roughness of less than 10 nm despite presenting a macroscopically mirrorlike surface. The average refractive index may be affected or reduced somewhat by the volume ratio of the surface roughness to film bulk.[33)] This may occur, as shown in Fig. 6, if the volume ratio of roughness increases non-negligibly with decreasing film thickness. However, these mechanisms are speculative without clear theoretical or experimental evidence. In the future, we will investigate and discuss these mechanisms further.

5. Conclusions

In this study, we investigated the dependences of the deposition rate of SiO_2 films and residual OH content in the deposited films on the concentration of TCE, which was added during the deposition, mainly at temperatures below 200 ^{o}C, with the reactant gases SO and O_3. At the constant TCE concentration of 0.25 mol/m^3, the deposition rate increases with deposition temperature up to 200 or 220 ^{o}C, but above that temperature, the deposition rate becomes saturated or decreases. Additionally, the deposition rate depends on the TCE concentration and is minimum at a concentration of ~0.4 mol/m^3. The results of the deposition temperature and TCE concentration dependences can be explained by the concepts of surface and gas-phase reactions. Experimentally, we also

1 revealed that the thickness profile is strongly affected by the gas-phase reaction, in
2 which the TCE vapor was blown directly onto the substrate surface, where it mixed with
3 SO and O_3. Furthermore, it was found that adding TCE vapor reduces residual OH
4 content in the low-temperature deposition SiO_2 film because the TCE enhances the
5 dehydration reaction. It is expected from these results that this TCE effect could be used
6 for other deposition methods using organic deposition sources.
7
8 **Acknowledgment**

9 This research is partially supported by JSPS KAKENHI Grant Number JP16K06257.
10
11 **Appendix**

12 The saturated vapor pressure P_{SO} (Pa) of $C_{10}H_{30}O_5Si_5$ is given by the equation

13 $$\ln(P_{SO}) = \mathrm{A} + \frac{\mathrm{B}}{T} + \mathrm{C}\cdot \ln T + \mathrm{D}\cdot T^{E} \;, \qquad \text{(A·1)}$$

14 where T is SO temperature (K), A = 94.421, B = -10153, C = -10.031, D = 7.47649×
15 10^{-18}, and E = 6.[34] The saturated vapor pressure P_{TCE} (Pa) of TCE is given by the
16 equation

17 $$\ln(P_{\mathrm{TCE}}) = 5\cdot \ln 10 \times [\mathrm{A} - \mathrm{B}/(T + \mathrm{C})], \qquad \text{(A·2)}$$

18 where T is TCE temperature (K), A = 3.55346 , B = 974.538, and C = -85.811.[35] This is
19 the Antoine equation with coefficients calculated from McDonald's data.[36]
20 The flow rates of SO (F_{SO}) and TCE (F_{TCE}) in the tube and before entering the
21 reaction chamber are calculated using the equations

22 $$F_{SO} = \frac{P_{\mathrm{SO}}\cdot F_{\mathrm{N2}}(\mathrm{SO})}{P_0 - P_{\mathrm{SO}}} \;, \qquad \text{(A·3)}$$

23 $$F_{\mathrm{TCE}} = \frac{P_{\mathrm{TCE}}\cdot F_{\mathrm{N2}}(\mathrm{TCE})}{P_0 - P_{\mathrm{TCE}}}, \qquad \text{(A·4)}$$

respectively. In this calculation, we assumed that the bubbling chambers of SO and TCE are in atmospheric pressure P_0 of 1 atm = 1.01×10^5 Pa, and that each flow rate is proportional to the saturation pressure of SO or TCE.

Using the same assumption for the reaction chamber, the SO (C_{SO}) and TCE (C_{TCE}) concentrations in the reaction chamber are calculated using the equations

$$C_{SO} = \frac{P'_{SO}}{RT_c} = \frac{P_0 \cdot F_{SO}}{RT_c \sum F} , \quad (A\cdot5)$$

$$C_{TCE} = \frac{P'_{TCE}}{RT_c} = \frac{P_0 \cdot F_{TCE}}{RT_c \sum F} , \quad (A\cdot6)$$

respectively, where $P'_{SO} = \frac{P_0 \cdot F_{SO}}{\sum F}$ and $P'_{TCE} = \frac{P_0 \cdot F_{TCE}}{\sum F}$ are the partial pressures of SO and TCE, respectively, T_c is temperature, ΣF is the sum of the flow rates of N_2, O_2, O_3, SO, and TCE in the reaction chamber, and R is the gas constant. Also, in this calculation, the ideal gas equation $PV = nRT$ is used, where P is pressure, V is volume, and n is the number of moles.

Using the O_3 concentration C'_{O3} before entering the reaction chamber, the O_3 concentration C_{O3} in the reaction chamber is calculated using the equation

$$C_{O3} = \frac{P_0 \cdot F_{O3}}{RT_c \sum F} = \frac{C'_{O2} \cdot F_{O3}}{\sum F} = \frac{C'_{O3} \cdot F_{O2}}{\sum F} , \quad (A\cdot7)$$

where F_{O2} and F_{O3} are the flow rates of O_2 and O_3, respectively, and C'_{O2} is the O_2 concentration at P_0 before flowing into the ozone generator. In this calculation, the relations $C'_{O2} = P_0/(RT_c)$ and $C'_{O2} : C'_{O3} = F_{O2} : F_{O3}$ are used.

The chemical reaction between silicone oil ($C_{10}H_{30}O_5Si_5$) and O_3 can be expressed by

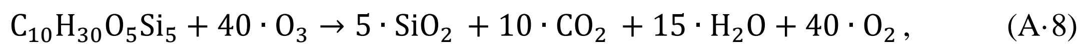

$$C_{10}H_{30}O_5Si_5 + 40 \cdot O_3 \rightarrow 5 \cdot SiO_2 + 10 \cdot CO_2 + 15 \cdot H_2O + 40 \cdot O_2 , \quad (A\cdot8)$$

assuming that the final products are stable molecules of SiO_2, H_2O, CO_2, and O_2 from O_3.

References

1) S. Higashi, D. Abe, S. Inoue, and T. Shimoda, Jpn. J. Appl. Phys. **40**, 4171 (2001).

2) M. M. Moslehi, R. A. Chapman, M. Wong, A. Paranjpe, H. N. Najm, J. Kuehne, R. L. Yeakley, and C. J. Davis, IEEE Trans. Electron Devices **39**, 4 (1992).

3) A. M. Mahajan, L. S. Patil, J. P. Bange, and D. K. Gautam, Vacuum **79**, 194 (2005).

4) Y. Nishi, T. Funai, H. Izawa, T. Fujimoto, H. Morimoto, and M. Ishii, Jpn. J. Appl. Phys. **32**, 6122 (1993).

5) N. Hirashita, S. Tokitoh, and H. Uchida, Jpn. J. Appl. Phys. **32**, 1787 (1993).

6) G. Mannino, R. Ruggeri, A. Alberti, V. Privitera, G. Fortunato, and L. Maiolo, Appl. Phys. Express **5**, 021103 (2012).

7) T. Toriyabe, K. Nishioka, and S. Horita, Proc. 13th Int. Display Workshops (IDW'06), 2006, p. 719.

8) S. Horita, K. Toriyabe, and K. Nishioka, Jpn. J. Appl. Phys. **48**, 035502 (2009).

9) H. Nakashima, K. Omae, T. Takebayashi, C. Ishizuka, and T. Uemura, J. Occup. Health **40**, 270 (1998).

10) S. Horita and P. Jain, Jpn. J. Appl. Phys. **56**, 088003 (2017).

11) T. Kawahara, A. Yuuki, and Y. Matsui, Jpn. J. Appl. Phys. **31**, 2925 (1992).

12) I. A. Shareef, G. W. Rubloff, M. Anderle, W. N. Gill, J. Cotte, and D. H. Kim, J. Vac. Sci. Technol. B **13**, 1888 (1995).

13) D. Cheng, K. Tsukamoto, H. Komiyama, Y. Nishimoto, N. Tokumasu, and K. Maeda, J. Appl. Phys. **85**, 7140 (1999).

14) S. Romet, M. F. Couturier, and T. K. Whidden, J. Electrochem. Soc. **148**, G82 (2001).

15) J. McMurry, *Fundamentals of Organic Chemistry* (Brooks/Cole, Belmont, CA, 2011) 7th ed., p. 339.

16) E. J. Kim and W. N. Will, J. Cryst. Growth **140**, 315 (1994).

17) K. Fujino, Y. Nishimoto, N. Tokumasu, and K. Maeda, J. Electrochem. Soc. **137**, 2883 (1990).

18) Y. Ikeda, Y. Numasawa, and M. Sakamoto, J. Electron. Mater. **19**, 45 (1990).

19) M. Ouyang, C. Yuan, R. J. Muisener, A. Boulares, and J. T. Koberstein, Chem. Mater. **12**, 1591 (2000).

20) Y. Nishi, T. Funai, H. Izawa, T. Fujimoto, H. Morimoto, and M. Ishii, Jpn. J. Appl. Phys. **31**, 4570 (1992).

21) M. Matsuura, Y. Hayashide, H. Kotani, and H. Abe, Jpn. J. Appl. Phys. **30**, 1530 (1991).

22) T. Ito, T. Matumoto, and K. Nishioka, Surf. Coatings Technol. **215,** 447 (2013).

23) P. Jaint and S. Horita, Proc. 21st Int. Workshop Active-Matrix Flatpanel Displays and Devices (AM-FPD), 2017, p. 285.

24) F. L. Galeener, Phys. Rev. B **19**, 4292 (1979).

25) P. G. Pai, S. S. Chao, Y. Takagi, and G. Lucovsky, J. Vac. Sci. Technol. A **4**, 689 (1986).

26) G. Lucovsky, M. J. Manitini, J. K. Srivastava, and E. A. Irene, J. Vac. Sci. Technol. B **5**, 530 (1987).

27) J. T. Fitch, G. Lucovsky, E. Kobeda, and E. A. Irene, J. Vac. Sci. Technol. B **7**, 153 (1989).

28) M. Yoshimaru and T. Yoshie, J. Electrochem. Soc. **145**, 2847 (1998).

29) N. Hirashita, S. Tokitoh, and H. Uchida, Jpn. J. Appl. Phys. **32**, 1787 (1993).

30) K. Murase, N. Yabumoto, and Y. Komine, J. Electrochem. Soc. **140**, 1722 (1993).

31) K. E. Oughstun and N. A. Cartwright, Opt. Express **11**, 1541 (2003).

32) L. Bányai and P. Gartner, Phys. Rev. B **29**, 728 (1984).

33) K. Imamura, D. Irishika, and H. Kobayashi, J. Appl. Phys. **121**, 013107 (2017).

34) D. N. Brooke, M. J. Crookes, D. Gray, and S. Robertson, Environmental Risk Assessment Report: Decamethylcyclopentasiloxane (Environment Agency, Bristol, U.K., 2009) p. 17.

35) NIST Chemistry WebBook, SRD 69 (National Institute of Standards and Technology, Gaithersburg, MD, 2016) [http://webbook.nist.gov/cgi/cbook.cgi?ID=C79016&Mask=4&Type=ANTOINE&Plot=on].

36) H. J. McDonald, J. Phys. Chem. **48**, 47 (1944).

Figure Captions

Fig. 1. (Color online) Schematic diagrams of the whole APCVD system (a) and the local line of the direct TCE flow (b) used in this research. In (a), the N_2 gas flow rate is 0.25 or 0.35 lm for SO ($C_{10}H_{30}O_5Si_5$) and the substrate temperatures range from 160 to 260 ^oC. The TCE concentration is varied from ~0.10 to ~0.7 mol/m^3 by controlling the TCE temperature from 5 to 32 ^oC and the N_2 gas flow rate, F_{N2}(TCE), from 0.03 to 0.1 lm for TCE bubbling. The flow of the TCE vapor was divided into two lines with a three-way valve: directly to the substrate or to the chamber bottom.

Fig. 2. (Color online) Typical FT-IR spectra of silicon oxide films deposited with and without TCE, where the TCE concentration is 0.25 mol/m^3. The N_2 gas flow rates for bubbling SO, F_{N2}(SO), are 0.25 (with TCE) and 0.35 (with and without TCE) lm.

Fig. 3. (Color online) Deposition temperature dependences of deposition rate obtained with and without TCE, where the temperatures range from 160 to 260 ^oC, and TCE concentration is 0.25 mol/m^3. F_{N2} (SO) with and without TCE are 0.25 and 0.35, and 0.35 lm, respectively. The plots and error bars indicate the averages and deposition rate ranges, respectively, among 6 measurement points for the two samples.

Fig. 4. (Color online) Dependence of deposition rate on TCE concentration for the F_{N2}(SO) of 0.35 (circles) and 0.25 (triangles) lm at the deposition temperature of 200 ^oC. The dotted line indicates the deposition rate without TCE as a reference.[23)] The plots and error bars have the same meanings as those in Fig. 3.

1

2 Fig. 5. (Color online) Dependence of deposition rate on relative OH content in the

3 deposited films for F_{N2}(SO) = 0.25(closed triangles) and 0.35(closed circles) lm with

4 TCE. As a reference, the open circle indicates the data without TCE. The thick broken

5 line is a guide for the eye. The plots and error bars indicate the averages and ranges of

6 ratios, respectively, among two or more measurement samples.[23)]

7

8 Fig. 6. (Color online) Film thickness *d* (closed) and refractive index *n* (open) profiles as

9 functions of the distance x from the tube outlet for the TCE flow rates of 0.0034

10 (circles) and 0.00065 (triangles). The deposition time is 10 min, the deposition

11 temperature is 200 ^{o}C, and the N_2 gas flow rate for bubbling SO, F_{N2}(SO), is 0.35 lm.

12

13 Fig. 7. Nomarsk optical micrographs of the surface regions at x = ~10 (a) and ~40 mm

14 (b) of the sample with the TCE flow rate = 0.0034 lm in Fig. 6.

15

16 Fig. 8. (Color online) Deposition model of SiO_2 film, focusing on the TCE-enhanced

17 dehydration reaction at the substrate surface. Enhanced dehydration reactions may

18 reduce the number of unreacted OH bonds in deposited SiO_2 films.

1
2
3
4
5
6
7
8
9
10
11
12
13
14
15
16
17
18
19
20
21
22
23

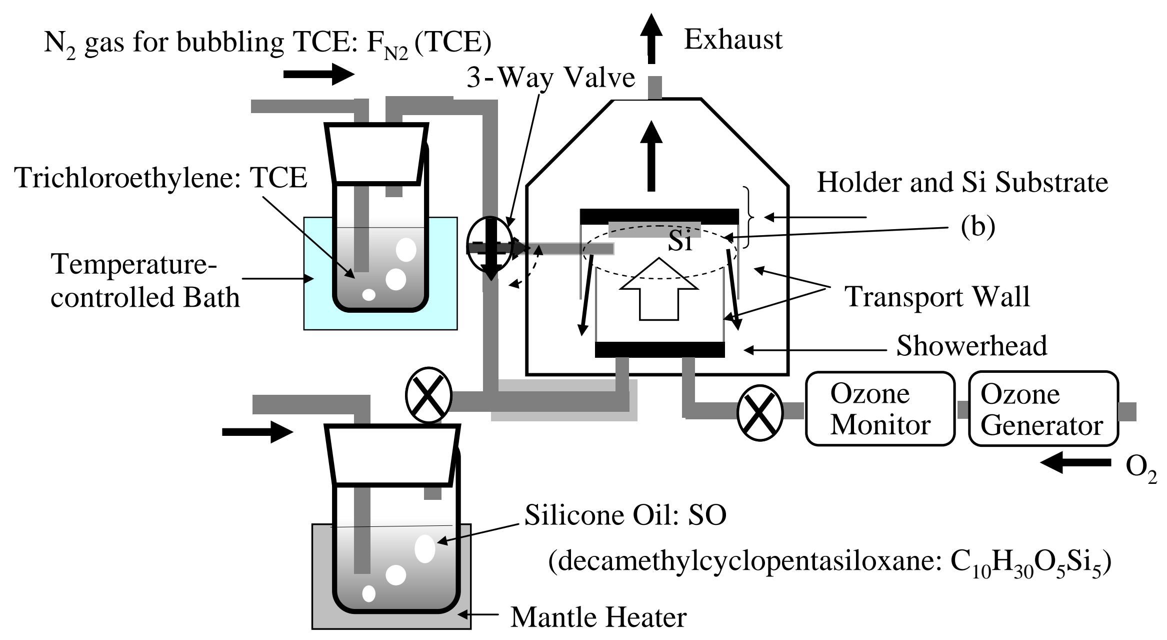

24 **Fig. 1(a)** **JJAP, S. Horita et al.**

1
2
3
4
5
6
7
8
9
10
11
12
13
14
15
16
17
18
19
20
21
22
23

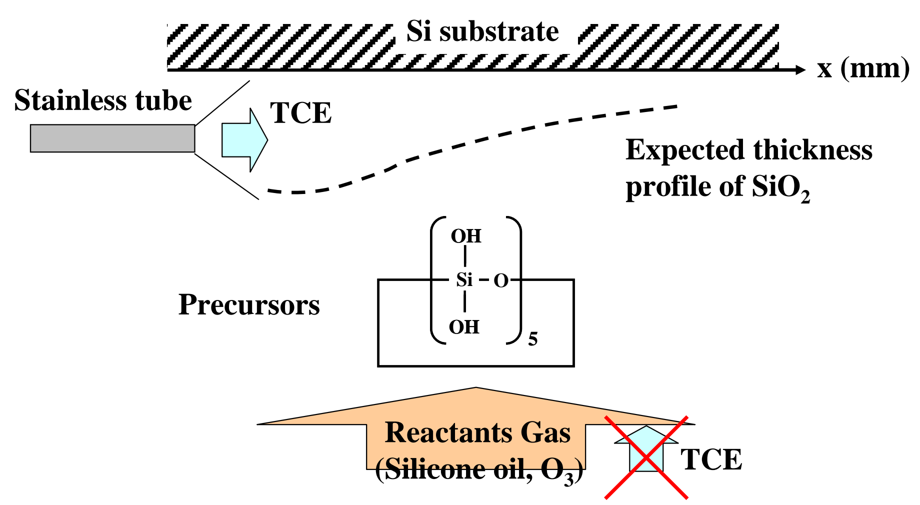

24 **Fig. 1(b)** **JJAP, S. Horita et al.**

1
2
3
4
5
6
7
8
9
10
11
12
13
14
15
16
17
18
19
20
21
22
23

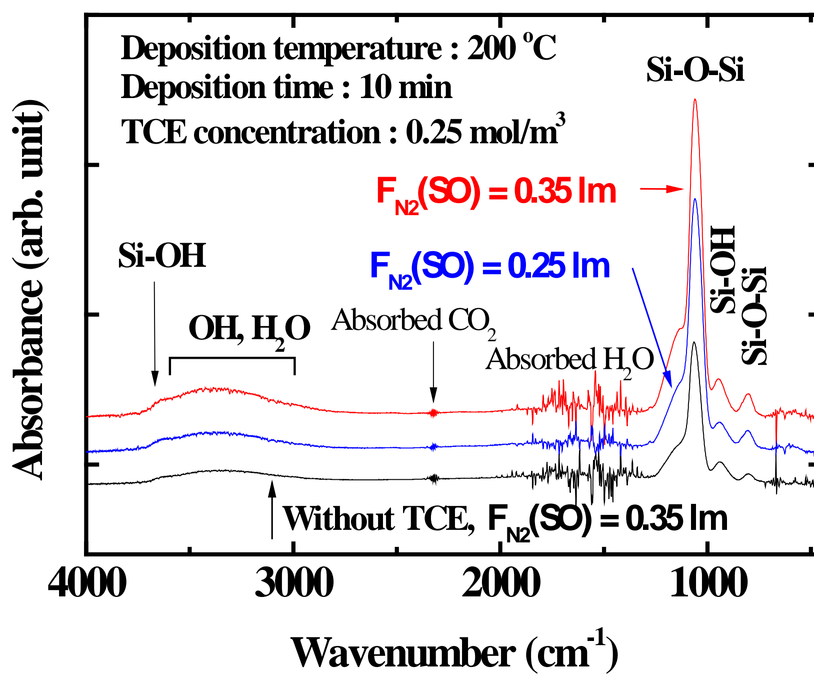

24 **Fig. 2** **JJAP, S. Horita et al.**

1
2
3
4
5
6
7
8
9
10
11
12
13
14
15
16
17
18
19
20
21
22
23

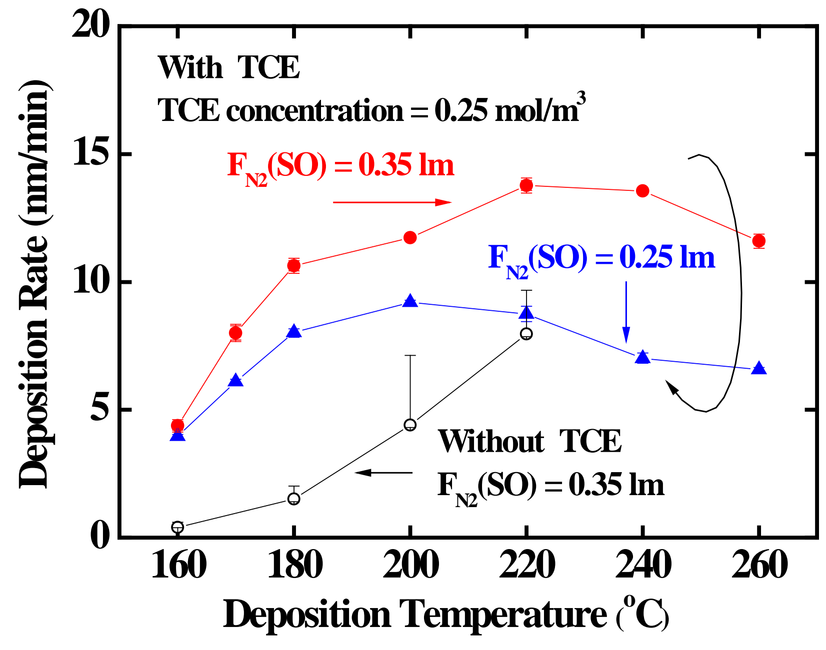

24 **Fig. 3** **JJAP, S. Horita et al.**

1
2
3
4
5
6
7
8
9
10
11
12
13
14
15
16
17
18
19
20
21
22
23

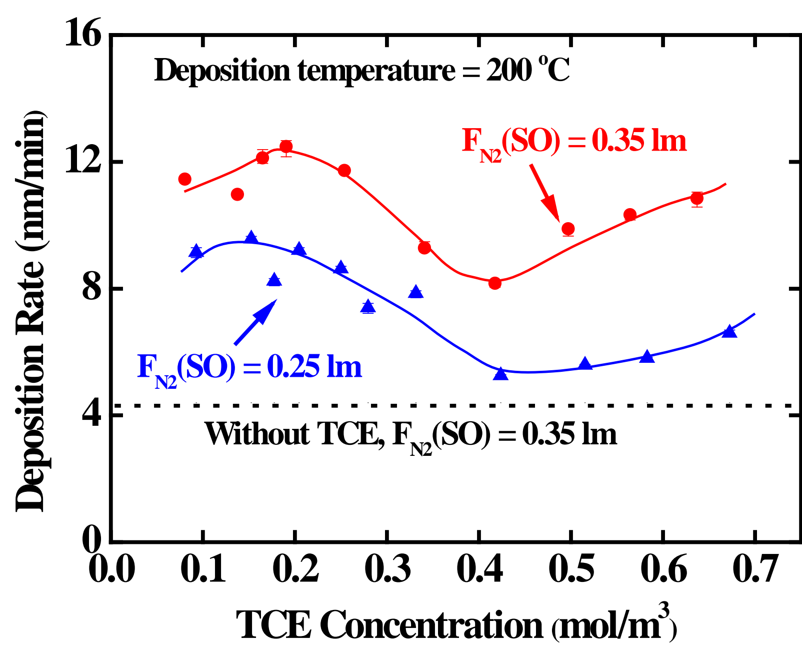

24 **Fig. 4** **JJAP, S. Horita et al.**

1
2
3
4
5
6
7
8
9
10
11
12
13
14
15
16
17
18
19
20
21
22
23

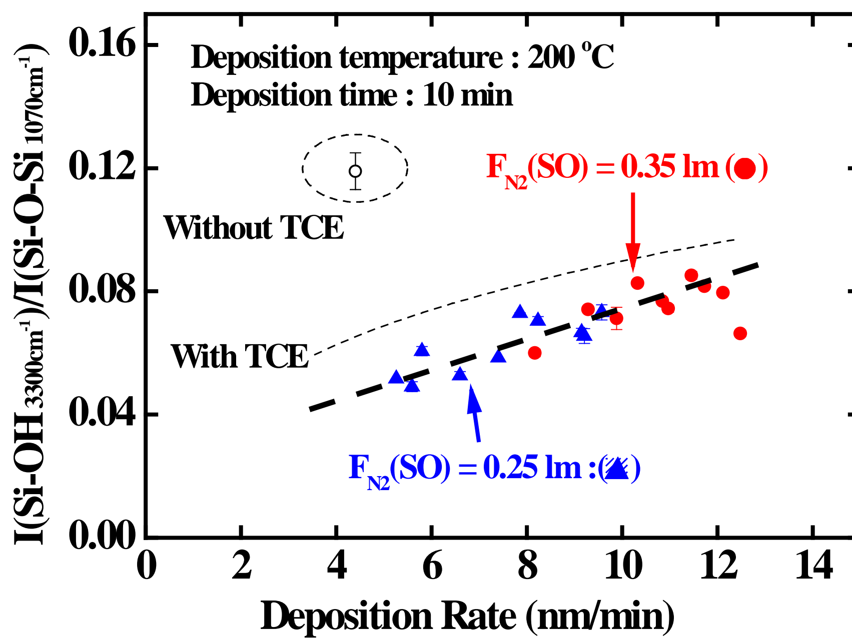

24 **Fig. 5** **JJAP, S. Horita et al.**

1
2
3
4
5
6
7
8
9
10
11
12
13
14
15
16
17
18
19
20
21
22
23

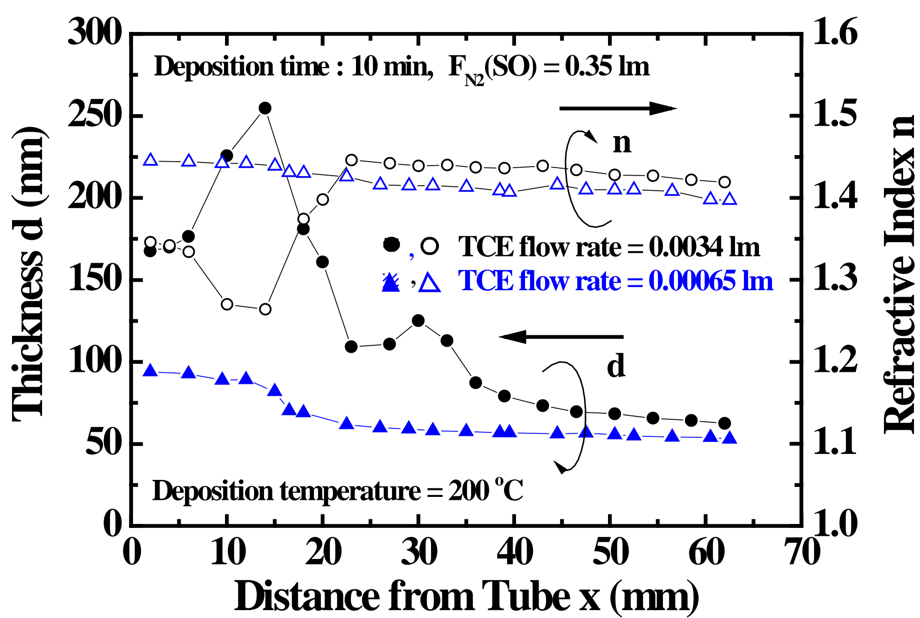

24 **Fig. 6** **JJAP, S. Horita et al.**

1
2
3
4
5
6
7
8
9
10
11
12
13
14
15
16
17
18
19
20
21
22
23

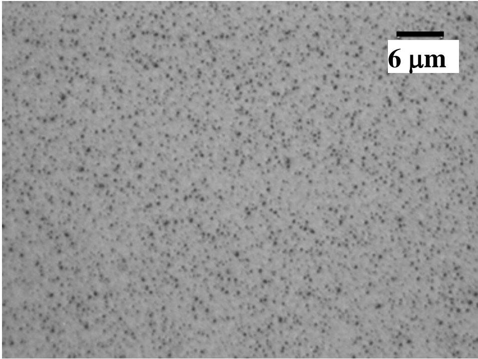

(a)

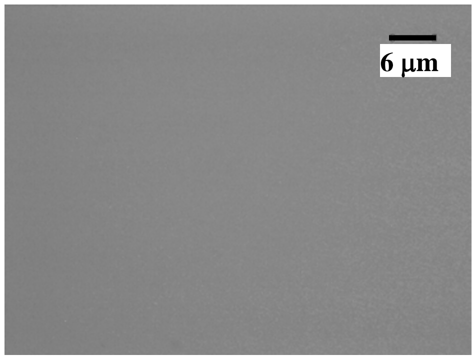

(b)

24 **Fig. 7** **JJAP, S. Horita et al.**

1
2
3
4
5
6
7
8
9
10
11
12
13
14
15
16
17
18
19
20
21
22
23

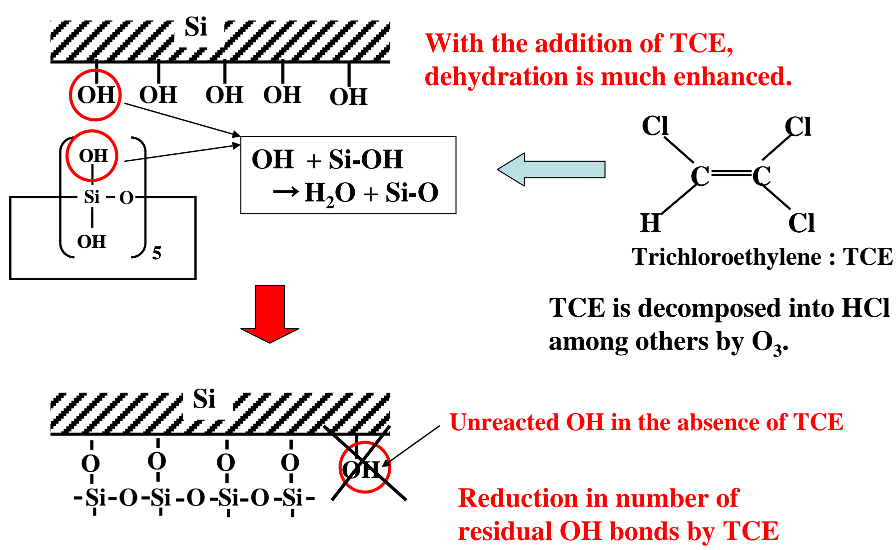

24 **Fig. 8** **JJAP, S. Horita et al.**